JURNAL REKAYASA PROSES
VOLUME 20, NUMBER 1, 2026, 001–011

RESEARCH ARTICLE

Hydrothermally synthesized hydroxyapatite from ale-ale shells as a bone graft material alternative

Tyas Galuh Amelia[1], Maulana Irfan Edri Prasetyo[1], Lalak Tarbiyatun Nasyin Maleiva[1,*], Adhityawarman[2], Syahrul Khairi[1]

[1]Department of Chemical Engineering, Faculty of Engineering, Tanjungpura University, Pontianak, 78124, Indonesia
[2]Department of Chemistry, Faculty of Mathematics and Natural Sciences, Tanjungpura University, Pontianak, 78124, Indonesia

Received 16 April 2025; revised 07 May 2025; accepted 26 February 2026

This graphical abstract was generated using AI-based image generation tools for conceptual illustration only.

OBJECTIVES Ale-ale shells (*Meretrix meretrix*), a locally abundant shellfish waste in West Kalimantan, Indonesia, were investigated as a sustainable calcium precursor for the hydrothermal synthesis of hydroxyapatite ($Ca_{10}(PO_4)_6(OH)_2$), the primary inorganic constituent of bone widely used in graft applications. METHODS Synthesis was conducted under varying reaction times (16–24 hours) and temperatures (140–180°C). RESULTS FTIR and XRD analyses confirmed the formation of hexagonal-phase hydroxyapatite consistent with the JCPDS 09-0432 standard, with characteristic hydroxyl and phosphate functional groups detected and minor carbonate incorporation (1.00–1.52%), remaining well below the 8% limit for bone implant applications. The optimum condition was identified at 160°C for 20 hours, yielding nano-scale hydroxyapatite (14.50 nm) with high crystallinity (98.90%), satisfying ISO 13779 requirements. CONCLUSIONS These findings highlight the potential of ale-ale shell-derived hydroxyapatite as a viable, locally sourced alternative to imported biomaterials while supporting the sustainable valorization of Indonesian shellfish waste.

KEYWORDS Bone graft; biowaste valorization; calcium phosphate; hydrothermal synthesis; hydroxyapatite; *Meretrix meretrix*

1. INTRODUCTION

Bone defects resulting from trauma, degenerative diseases, and surgical resection represent a major clinical and socioeconomic burden, driving sustained demand for reliable bone substitute materials worldwide (Johansson et al. 2015). Treatment strategies commonly involve the transplantation of bone grafts or implantation of synthetic biomaterials to restore structural integrity and function of the affected tissue (Anisah et al. 2018). Among available options, natural bone grafts such as autografts and allografts remain the gold standard; however, they are constrained by limited donor availability, donor site morbidity, immune rejection, and risk of disease transmission. These limitations have intensified research efforts toward synthetic alternatives, particularly calcium phosphate-based biomaterials such as hydroxyapatite.

Hydroxyapatite (HAp, $Ca_{10}(PO_4)_6(OH)_2$) is the primary inorganic constituent of human bone, comprising approximately 65% of bone mineral by weight (Harahap et al. 2015). Its inherent biocompatibility, bioactivity, and osteoconductivity make it a highly attractive material for bone graft applications (Sadat-Shojai et al. 2013). In Indonesia, however, hydroxyapatite remains largely imported, resulting in high costs that limit widespread clinical availability. Local shellfish waste presents a promising and sustainable calcium source for HAp synthesis, given Indonesia's substantial shellfish production of approximately 146,948 tons annually (Directorate General of Capture Fisheries 2021). Among these resources, ale-ale shells (*Meretrix meretrix*), a bivalve commonly harvested in Kalimantan, have been reported to contain high calcium oxide content following calcination (Oktaviani 2019). Despite this potential, ale-ale shells remain significantly underexplored as a precursor for hydroxyapatite synthesis. To the best of our knowledge, limited studies have systematically investigated the hydrothermal synthesis of hydroxyapatite using ale-ale shells as the sole calcium source, representing a clear gap in the utilization of Indonesian marine biowaste for biomedical applications.

Among various synthesis methods reported for hydroxyapatite production, including precipitation, sol–gel, and solid-state reaction, hydrothermal synthesis was selected in

*Correspondence: lalaktnm@teknik.untan.ac.id

this study due to its superior ability to produce highly crystalline, phase-pure particles under relatively moderate conditions using water as a solvent (Harahap et al. 2015). The quality of synthesized hydroxyapatite is evaluated based on several parameters, including Ca/P molar ratio, crystallinity, crystal size, phase purity compared to JCPDS 09-0432 standard data, and carbonate impurity content. However, hydrothermal synthesis is sensitive to processing parameters: insufficient temperatures lead to incomplete crystal formation, while excessively high temperatures may damage the crystal structure. Similarly, reaction time must be carefully controlled, as too short a duration results in incomplete crystallization, and too long a duration promotes the formation of secondary calcium phosphate phases (Berzina-Cimdina and Borodajenko 2012). Systematic optimization of these parameters is therefore essential to obtain HAp that conforms to the JCPDS 09-0432 standard and is suitable for bone graft applications.

While hydroxyapatite synthesis from bivalve shells has been reported using cockle (Azis et al. 2015) and green mussel (Rachmantio and Irfai 2023), as well as from other marine biowaste sources such as fish bones (Piccirillo et al. 2013) and sea urchin spines (Phatai et al. 2018), these studies predominantly employed co-precipitation methods, which tend to yield products with lower crystallinity and less controlled phase purity compared to hydrothermal approaches. Ale-ale shells (*Meretrix meretrix*) remain largely unexplored as a hydrothermal HAp precursor, and no prior study has systematically addressed the combined effects of reaction time and temperature on yield, carbonate content, crystallinity, and crystal size from this source. This represents a significant gap in both the utilization of Indonesian marine biowaste and the process optimization of biowaste-derived hydroxyapatite for biomedical applications.

This study therefore aims to address this gap by: (1) optimizing the hydrothermal reaction time and temperature for the synthesis of phase-pure hydroxyapatite from ale-ale shells, (2) characterizing the physicochemical properties of the synthesized HAp including functional groups, crystallinity, and crystal size, and (3) evaluating its potential as a bone graft material candidate through comparison with commercial hydroxyapatite and the ISO 13779 standard. This work contributes to the development of affordable, locally sourced biomaterials and demonstrates the feasibility of converting Indonesian shellfish waste into high quality hydroxyapatite suitable for further biomedical evaluation.

2. RESEARCH METHODOLOGY

2.1 Materials

The raw material used in this study was ale-ale shells obtained from Ketapang, which were subsequently calcined to produce CaO. Ammonium hydrogen phosphate ($(NH_4)_2HPO_4$, analytical grade) was commercially obtained and used without further purification. Ammonium hydroxide (NH_4OH, analytical grade) was used as a pH adjuster. Distilled water was used throughout the synthesis.

2.2 Equipments

The primary equipment used includes a hydrothermal reactor, furnace, oven, 200 mesh sieve, and pH meter (1).

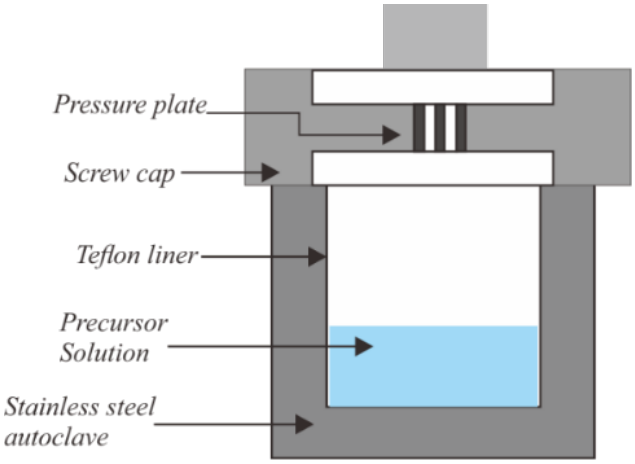

FIGURE 1. Hydrothermal reactor.

2.3 Procedures

2.3.1 Preparation of ale-ale shells

Ale-ale waste shells were washed and dried under sunlight to remove remaining dirt and moisture. The dried shells were ground and sieved using a 200-mesh sieve to obtain an average particle size of 200 mesh. The shells were then calcined in a furnace at 900°C for 4 h to convert $CaCO_3$ into CaO.

2.3.2 Synthesize of hydroxyapatite

Each synthesis condition was performed as a single independent batch. A total of nine batches were synthesized, corresponding to all combinations of three reaction temperatures (140°C, 160°C, and 180°C) and three reaction times (16, 20, and 24 hours), each using 10 g CaO and 14.26 g $(NH_4)_2HPO_4$ as precursors in approximately 130 mL total volume of distilled water.

The Ca/P molar ratio was fixed at 1.67, which corresponds to the stoichiometric composition of phase-pure hydroxyapatite ($Ca_{10}(PO_4)_6(OH)_2$). This ratio is widely recognized as the theoretical standard for stoichiometric HAp and is a crit-

FIGURE 2. Ale-ale shells calcination result.

TABLE 1. Percentage of elements and oxides in ale-ale shells.

Elements	Percentage (%)	Oxide Molecules	Percentage (%)
Ca	94.42	CaO	93.44
Fe	2.08	Fe2O3	1.93
Si	0.87	SiO2	1.59
In	0.87	In2O3	0.71
P	0.47	P2O5	0.89
Sr	0.45	SrO	0.34
Al	0.37	Al2O3	0.60
Ti	0.22	TiO	0.23
Ag	0.17	Ag2O	0.14
Others	0.03	Others	0.07

ical parameter in controlling phase purity of the synthesized product (Sadat-Shojai et al. 2013).

The precursor solutions were combined, and the pH was adjusted to 11 by dropwise addition of NH_4OH. The mixture was subsequently transferred into a hydrothermal reactor and heated at the specified temperatures (140, 160, 180°C) for the designated reaction times (16, 20, 24 hours). After hydrothermal treatment, the reactor was allowed to cool naturally to room temperature. The resulting precipitate was washed with distilled water until neutral pH was achieved, filtered, and dried at 110°C for 5 hours to obtain the final white powder product.

2.3.3 Characterizations

The synthesized hydroxyapatite samples were characterized using Fourier Transform Infrared (FTIR) spectroscopy to identify the functional groups present in the material. The optimal reaction time was determined based on the product yield, and the carbonate content was estimated using the FTIR absorbance ratio method proposed by Featherstone et al. (1984).

X-ray diffraction (XRD) analysis was performed to determine the crystal structure, crystallite size, and degree of crystallinity. The crystallite size was calculated using the Scherrer equation. The obtained data were processed using OriginPro software.

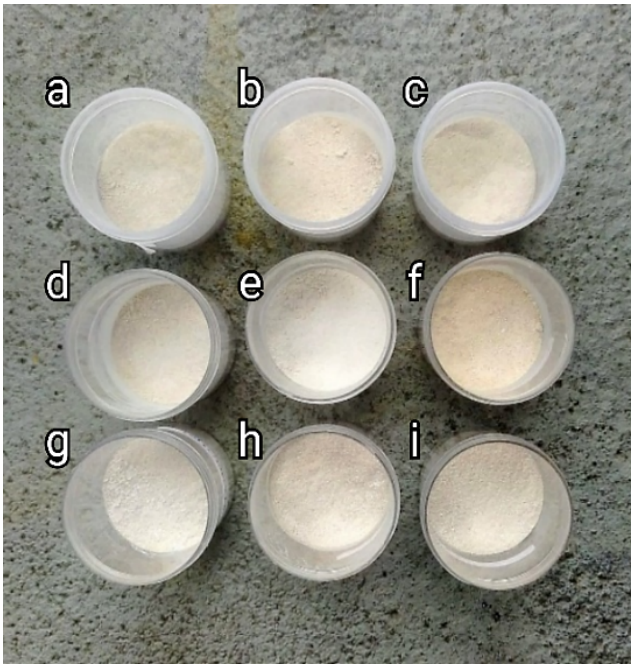

FIGURE 3. Hydroxyapatite synthesis results at (a) 140°C; 16 hours, (b) 160°C; 16 hours, (c) 180°C; 16 hours, (d) 140°C; 20 hours, (e) 160°C; 20 hours, (f) 180°C; 20 hours, (g) 140°C; 24 hours, (h) 160°C; 24 hours, and (i) 180°C; 24 hours.

3. RESULTS AND DISCUSSION

3.1 Sample preparation

The sieved ale-ale shells were calcined for 4 hours at 900°C. Calcination aims to release gases in the form of carbonate or hydroxide to produce material in oxide form. The decomposition reaction of calcium carbonate into calcium oxide (CaO) is shown below:

$$CaCO_{3(s)} \rightarrow CaO_{(s)} + CO_{2(g)} \quad (1)$$

After the calcination process, the mass decreased from 137 grams to 91.03 grams. The reduction in mass resulted from the release of impurities present in the ale-ale shells. Additionally, the color of the sample changed from dark gray to whitish gray, which was a result of the loss of water content in the sample after the calcination process. The results of the calcination process are displayed in Figure 2.

After calcination, clam shells were analyzed by XRF to determine the amount of CaO in the shells. Table 1 displays the XRF characterization results for the major components in ale-ale shells.

According to the XRF results in Table 1, the calcined ale-ale shells exhibited a high calcium content of 94.42%, corresponding to 93.44% CaO. Minor elements such as Fe (2.08%), Si, In, P, Sr, Al, Ti, and Ag were also detected, indicating the presence of natural mineral impurities in the shell material. The Ca content obtained in this study was slightly higher than that reported by Oktaviani (2019), who observed 89.88% Ca and 87.13% CaO in calcined ale-ale shells at 900°C. The Fe content in the present study is also comparable to their reported value of 2.00%. The high calcium content confirms that ale-ale shells are a promising raw material for hydroxyapatite synthesis.

3.2 Synthesize of hydroxyapatite

Hydroxyapatite was successfully synthesized via hydrothermal processes using ale-ale clam shells. The resulting prod-

TABLE 2. Hydroxyapatite synthesis yield.

Reaction time (hours)	Yields (%)		
	140°C	160°C	180°C
16	52.18	52.88	47.85
20	52.43	54.08	52.14
24	51.44	51.60	51.40

uct is a fine, odorless white powder. Although stoichiometrically pure hydroxyapatite appears white, products synthesized from natural biowaste sources may exhibit slight color variations due to residual impurities. The gray hue observed in some samples is attributed to incomplete calcination of $CaCO_3$, while the yellowish tint is associated with trace iron oxide impurities present in the raw material (Tang et al. 2023; Ishikawa and Ogawa 2004).

In this study, there were some samples that had a slightly yellowish-white color. Impurities present in hydroxyapatite, although in small quantities, could be a potential cause for the yellow tint in the color of hydroxyapatite. Among the impurities identified in the sample history, iron is one of the most common. The calcined ale-ale shells containing 2.08% iron ions or traces of iron oxide may cause a yellowish hue. When iron is present in hydroxyapatite, its ions or oxide particles interact with light, leading to reflection, absorption, or refraction by the iron impurity. This can shift the wavelength of the reflected light, resulting in the yellowish color seen in hydroxyapatite (Tang et al. 2023). The synthesis results are presented in Figure 3 and the resulting yields in Table 2.

3.3 The Effect of Reaction Time in Hydrothermally Synthesized Hydroxyapatite

The average yield of hydroxyapatite across all synthesis conditions was approximately 50% of the total precursor mass used. This is attributed to product loss during the washing step, in which soluble by-products, primarily ammonium salts formed during the synthesis reaction, are dissolved and removed, while the insoluble hydroxyapatite precipitate is retained by filtration.

The yield trend observed across reaction times can be explained by nucleation and crystal growth kinetics. In the early stages of the hydrothermal reaction, calcium and phosphate ions accumulate in solution, progressively increasing the degree of supersaturation until spontaneous nucleation is triggered. Crystal nucleation and growth then occur simultaneously, gradually consuming the available ions and reducing supersaturation. In the final stage, crystal growth becomes the dominant process (Yusuf 2021). Beyond the optimum reaction time, the availability of calcium and phosphate ions in solution diminishes, reducing the sedimentation rate of hydroxyapatite particles and ultimately decreasing the product yield (Zhu et al. 2018). The FTIR spectra are displayed in Table 3.

FTIR characterization of all synthesized samples confirmed the presence of hydroxyl (OH^-) and phosphate (PO_4^{3-}) functional groups, which are characteristic of hydroxyapatite, alongside minor carbonate (CO_3^{2-}) impurities. The O-H absorption peak in the hydroxyl group is the most typical and easily recognized peak in the FTIR spectrum. This peak occurs due to the stretching of the bond between the oxygen (O) and hydrogen (H) atoms in the hydroxyl group (OH^-). The hydroxyl (OH^-) groups were detected at 2164, 2176, 3617, 3624, 3429, 3630, 3631, 3432 cm^{-1}. According to Berzina-Cimdina and Borodajenko (2012) and Castro et al. (2022), hydroxyl functional groups are usually found at 3700-2600 cm^{-1} and 2520-2075 cm^{-1} because these wavelengths are the typical bands of these groups. The main characteristic of the O-H absorption peak of alcohol is the narrow and short absorption peak. O-H absorption peaks also often appear as double peaks. This is caused by hydrogen bonding interactions between molecules containing hydroxyl groups. Hydrogen bonding interactions can cause the appearance of double peaks in the spectrum and a shift in the O-H peak. However, this peak shift can occur due to the chemical environment and the hydrogen bonds formed with phosphate, carbonate, or other components in the HAp. The O-H absorption peak may appear as a double peak due to variations in the hydrogen bonds formed between hydroxyl groups of hydroxyapatite and other components in the structure. These hydrogen bond interactions can cause a shift and broadening of the O-H absorption peak. Typically, stronger hydrogen bonds tend to cause the O-H peak to shift lower, i.e., below 3570 cm^{-1}.

The hydroxyapatite component can be identified from the phosphate functional group, which is one of the important components for bone (Ryu et al. 2019). The absorption peak of the phosphate group in FTIR tends to have a strong intensity. This is due to the presence of a strong bond between phosphorus and oxygen atoms in the phosphate group. Therefore, the phosphate absorption peak can be a clear and well-observed peak in the FTIR spectrum. The phosphate group is also the group that has the sharpest peak in hydroxyapatite compounds (Azis et al. 2015). The phosphate group (PO_4^{3-}) was found at 1024 cm^{-1}, 562 cm^{-1} and 424 cm^{-1}. This is in agreement with previous studies reporting that PO_4^{3-} vibrational peaks are typically observed in the range of 400–1100 cm^{-1} (Fadli et al. 2014; Sahadat Hossain and Ahmed 2023; Abifarin et al. 2019). These absorption bands correspond to the fundamental vibrational modes (v_1–v_4) of the tetrahedral PO_4^{3-} ion, where v_3 represents asymmetric stretching and v_4 corresponds to asymmetric bending vibrations. The FTIR characterization results show that the phosphate group (PO_4^{3-}) is characterized by a strong and sharp band.

The presence of hydroxyl and phosphate groups in the synthesized hydroxyapatite crystals indicates that the hydroxyapatite crystals have been successfully synthesized, while the presence of carbonate groups is at a low intensity. The carbonate group (CO_3^{2-}), which is an impurity, was detected at 1417 cm^{-1}. Carbonate substitution in hydroxyapatite is typically observed in the region of 1400–1450 cm^{-1}, corresponding to the v_3 asymmetric stretching vibrational mode

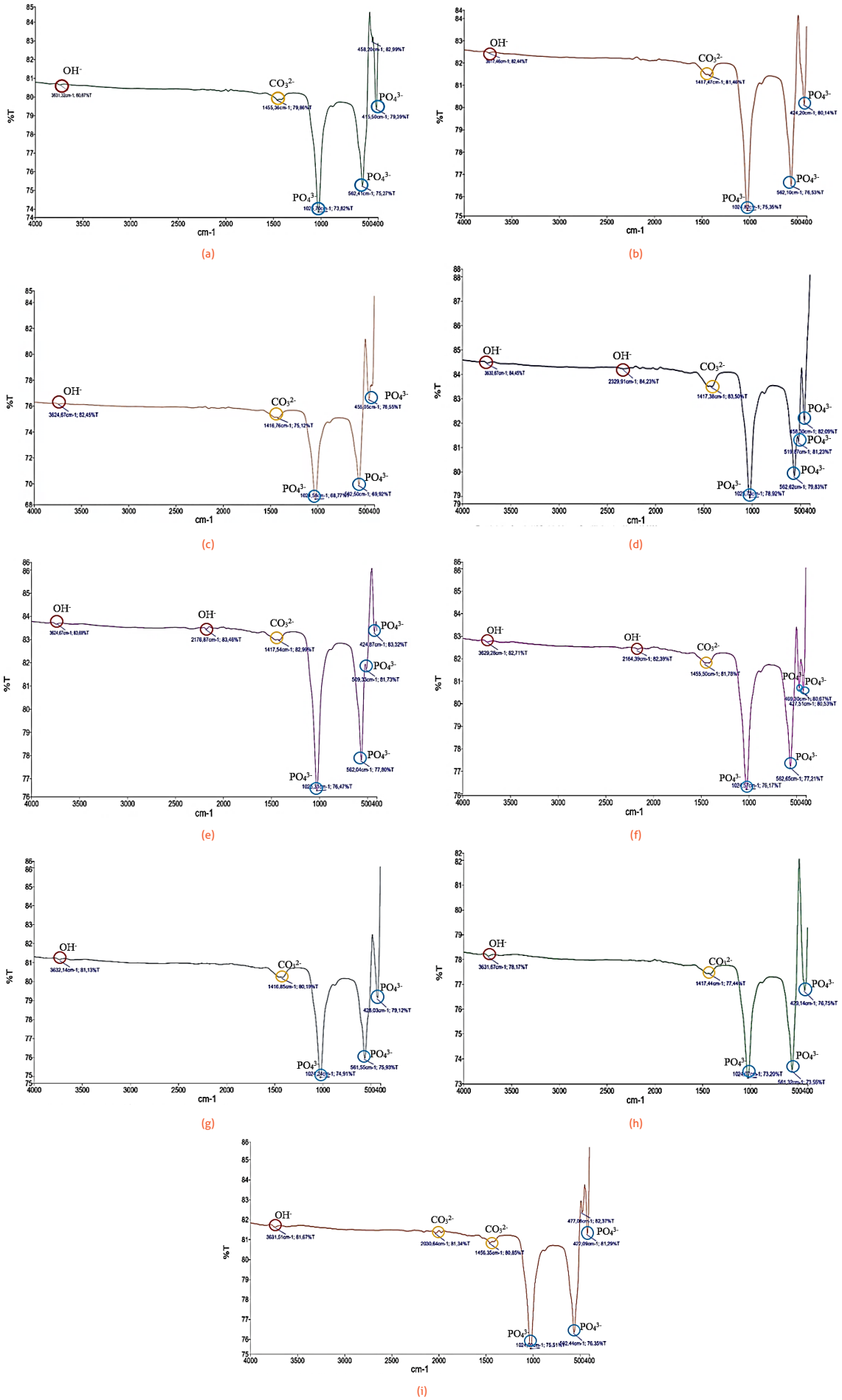

FIGURE 4. Hydroxyapatite synthesis results at (a) 140°C; 16 hours, (b) 160°C; 16 hours, (c) 180°C; 16 hours, (d) 140°C; 20 hours, (e) 160°C; 20 hours, (f) 180°C; 20 hours, (g) 140°C; 24 hours, (h) 160°C; 24 hours, and (i) 180°C; 24 hours.

TABLE 3. IR Wavelength Range.

Conditions	Wavelength Range (cm-1)					
	OH-	PO_4^{3-}	CO_3^{2-}	OH^-	PO_4^{3-}	CO_3^{2-}
16 hours; 140 °C				3631	1025, 562, 415	1455
16 hours; 160 °C				3617	1024, 562, 424	1417
16 hours; 180 °C				3624	1024, 562, 455	1416
20 hours; 140 °C				3630, 2329	1024, 562, 519, 458	1417
20 hours; 160 °C	3700-2600 and 2520-2075	400-1050	1390-1630, 2030, and 2032	3624, 2176	1025, 562, 509, 424	1417
20 hours; 180 °C				3629, 2164	1024, 562, 469, 427	1455
24 hours; 140 °C				3632	1024, 561, 428	1416
24 hours; 160 °C				3631	1024, 561, 429	1417
24 hours; 180 °C				3631	1024, 562, 477	1456, 2030

of type B CO_3^{2-} in the apatite lattice (Fleet and Liu 2004, 2007). The presence of this band indicates partial incorporation of carbonate ions during the hydrothermal process through substitution at phosphate sites (type B substitution), which is commonly reported in carbonated hydroxyapatite. Similar observations have also been reported by Sahadat Hossain and Ahmed (2023). The presence of impurities in the form of carbonates is caused by the reaction of CO_2 in the reactor atmosphere with hydroxyapatite forming precursors during the synthesis process due to the heat treatment provided (Sulistyawati and Siregar 2019). This causes CO_2 to interact with distilled water (H_2O), which is the solvent in the synthesis process, resulting in the formation of carbonate anions (CO_3^{2-}), which eventually mix into the synthesized hydroxyapatite crystal structure.

Among all synthesis conditions, samples prepared at a reaction time of 20 hours exhibited a greater number of hydroxyl and phosphate absorption peaks, suggesting more complete HAp formation at this optimum reaction time. The appearance of more hydroxyl group absorption peaks at a reaction time of 20 hours is due to the interaction of hydrogen bonds between molecules containing hydroxyl groups. In FTIR spectra, hydrogen bond interactions can produce two absorption peaks associated with strong and weak hydrogen bonds. The strong hydrogen bond absorption peak usually appears at higher wave numbers and has a higher intensity. Absorption peaks of weak or broken hydrogen bonds may appear at lower wave numbers and have lower intensities. Meanwhile, the appearance of more phosphate absorption peaks at a reaction time of 20 hours is due to the substitution of CO_3^{2-} ions by PO_4^{3-} when the optimum reaction time is reached. This substitution causes a change in the absorption peak associated with the phosphate group in the FTIR spectrum. This substitution can affect the bond strength and structure of the phosphate group, resulting in additional absorption peaks (Gheisari et al. 2015).

However, there is an anomaly that occurs in hydroxyapatite synthesized at a temperature of 180°C for 24 hours, there is a peak found at 2030 cm^{-1} that is identified as a carbonate group. This is due to the fact that the hydrothermal process is too long, excessive reaction time provides an opportunity for CO_2 interaction with H_2O in hydroxyapatite. The longer the reaction time, the more intense the interaction between CO_2 and H_2O, can produce more carbonate groups seen in the IR spectra. In addition, an increase in temperature beyond the optimum temperature will increase the rate of the carbonation reaction. This can result in the replacement of hydroxyl groups in hydroxyapatite with carbonate groups, increasing the number of carbonate groups formed in the crystal structure. The presence of carbonate groups (CO_3^{2-}) are not necessarily a negative indication. Human bones have a component in the form of carbonate that naturally replaces phosphate ions according to the equation $Ca_{10}(CO_3)_x(PO_4)_{6(2/3)x}(OH)_2$, or carbonated hydroxyapatite. However, since the presence of carbonate is an uncontrollable factor in this synthesis process, it can be categorized as an impurity. Other impurities detected are due to the history of raw materials, where the synthesis process uses natural materials that contain contaminating or undesirable components (Purwasasmita and Gultom 2008).

The carbonate content in the synthesized hydroxyapatite was estimated using the semi-quantitative FTIR method proposed by Featherstone et al. (1984). In this approach, the carbonate percentage is calculated from the extinction ratio between the carbonate absorption band at approximately 1415 cm^{-1} and the phosphate reference band at approximately 575 cm^{-1}. The carbonate content was determined using the following empirical equation:

$$\%\text{Carbonate} = 16.1 \times \left(\frac{E_{1415}}{E_{575}}\right) - 0.2 \quad (2)$$

Where the extinction value E is defined as:

TABLE 4. Estimated Carbonate percentage of synthesized hydroxyapatite.

Reaction time (hours)	Carbonate Quantity (%)		
	140°C	160°C	180°C
16	1.38	1.16	1.21
20	1.33	1.00	1.20
24	1.52	1.16	1.34

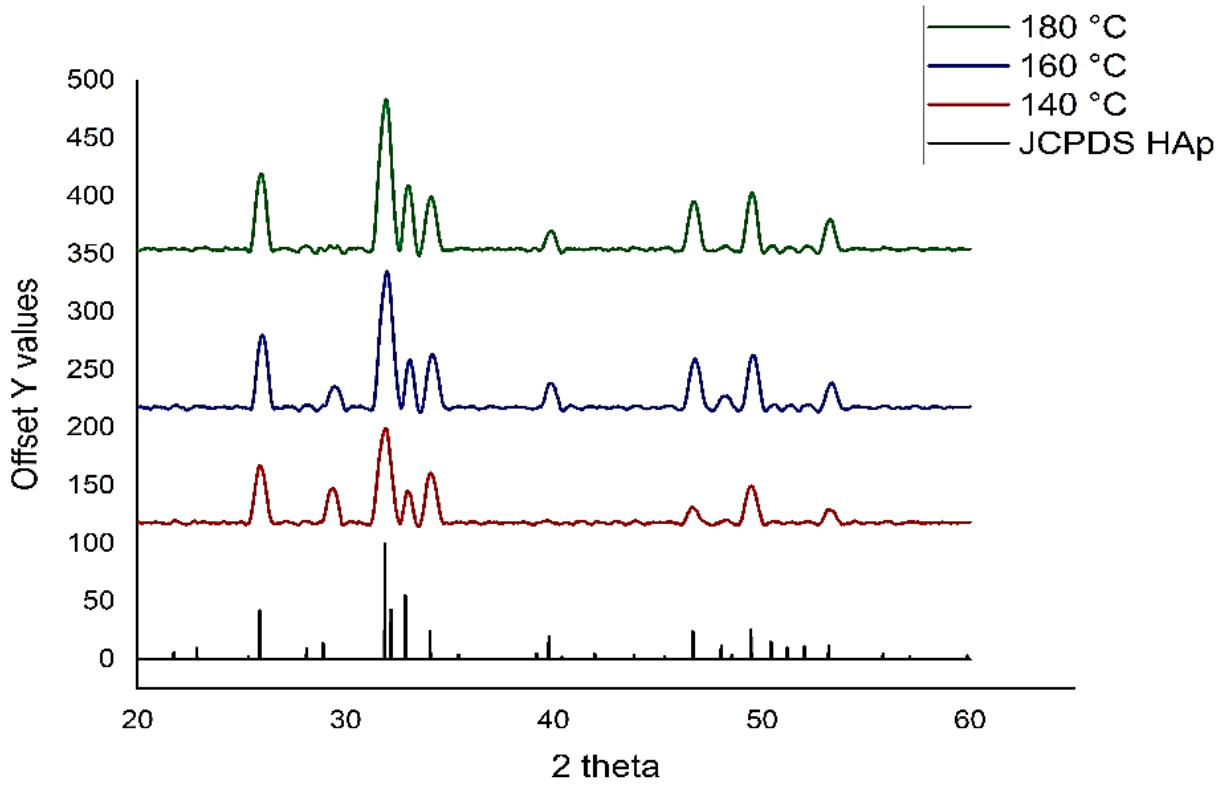

FIGURE 5. Hydroxyapatite diffractogram and JCPDS standard.

$$E = \log\left(\frac{T_2}{T_1}\right) \quad (3)$$

in which T_1 represents the peak transmittance and T_2 represents the baseline transmittance. The calculated extinction ratio was substituted into the empirical equation to estimate the relative carbonate percentage. Although this method does not provide absolute quantification, it has been widely applied for comparative evaluation of carbonate incorporation in hydroxyapatite. Future studies may incorporate thermogravimetric analysis (TGA) to further validate carbonate quantification.Table 4 presents the quantity of carbonate impurities found in the synthesis results.

The carbonate content across all synthesized samples was quantified and is presented in Table 4. The maximum allowable carbonate content for hydroxyapatite as bone implants is 8% (Castro et al. 2022), and all synthesized samples were found to be below this threshold. Longer treatment times can lead to increased carbonate ion diffusion into the hydroxyapatite crystal structure during the reaction, resulting in more carbonate in the synthesis results. In short, shorter treatment times can lead to incomplete crystallization of hydroxyapatite, causing incomplete and inhomogeneous crystal growth. Meanwhile, longer treatment times can lead to increased ion interactions in solution, allowing the formation of different calcium phosphate compounds, including monetite ($CaHPO_4$) (Earl et al. 2006).

From a mechanistic standpoint, carbonate incorporation in hydroxyapatite occurs through two distinct substitution mechanisms. In type A substitution, CO_3^{2-} replaces hydroxyl ions (OH^-) in the apatite channel sites, while in type B substitution, CO_3^{2-} replaces phosphate ions (PO_4^{3-}) at tetrahedral sites within the crystal lattice (Fleet and Liu 2004). The detection of the carbonate band at 1417 cm^{-1} in the present study, which falls within the characteristic v_3 asymmetric stretching region of type B carbonate (1400–1450 cm^{-1}), suggests that carbonate incorporation occurred predominantly via type B substitution (Fleet and Liu 2007). Type B substitution is particularly relevant from a biological perspective, as it closely mimics the carbonate substitution pattern found in natural human bone mineral, where approximately 4–8 wt% CO_3^{2-} is incorporated predominantly at phosphate sites (LeGeros 2002). This structural similarity to biological apatite is considered advantageous for bone graft applications, as carbonate substitution has been shown to increase the solubility and biodegradability of synthetic HAp, thereby facilitating osteoclast-mediated resorption and subsequent new bone formation (Barrère et al. 2006). In the present study, carbonate content ranged from 1.00–1.52%, which lies within the physiologically relevant range and well below the 8% maximum stipulated for bone implant applications (Castro et al. 2022). Therefore, the level of carbonate incorporation observed in this study may be regarded as a favorable characteristic that enhances the biomimetic nature of the synthesized hydroxyapatite, rather than a critical impurity.

An anomalous absorption peak at 2030 cm^{-1} was observed exclusively in the sample synthesized at 180°C for 24 hours. This band was attributed to carbonate-related species, consistent with reports of CO_3^{2-}-associated absorptions appearing in the 2000–2100 cm^{-1} region under prolonged thermal treatment conditions. The occurrence of this peak at the highest temperature–time combination investigated is in line with increased carbonation rates promoted by elevated temperature and extended exposure time, which intensify CO_2–H_2O interactions within the hydrothermal environ-

ment (Sulistyawati and Siregar 2019). This interpretation is supported by the slightly higher carbonate content (1.34%) measured under this condition (Table 4).

Nevertheless, absorptions in the 2000–2100 cm^{-1} region may also arise from atmospheric CO_2 adsorption during FTIR measurement or from minor surface impurities. Therefore, the definitive assignment of this band to carbonate incorporation requires complementary characterization techniques such as Raman spectroscopy or thermogravimetric analysis (TGA). Given that this condition was conducted as a single synthesis batch, the anomalous peak should be interpreted cautiously. Future investigations incorporating replicate syntheses and additional spectroscopic validation are recommended to confirm this observation.

3.4 The effect of temperature in hydrothermally synthesized hydroxyapatite

Temperature is a critical parameter in hydrothermal synthesis, directly influencing reaction kinetics, crystal growth, and the physicochemical properties of the resulting hydroxyapatite. However, high temperatures can also induce irregular crystal growth or even produce undesired products. Additionally, temperature also affects the chemical composition of the hydroxyapatite produced. Lower temperatures can lead to poor synthesis results, while too high a temperature can decompose the phosphate so that the resulting hydroxyapatite may contain different mineral phases. Temperature also impacts crystal size, with higher synthesis temperatures leading to smaller diameter crystals (Hokmabad et al. 2019). Therefore, XRD analysis was conducted to assess the compatibility of the synthesized hydroxyapatite compound with JCPDS standard data, crystallinity, and crystal size. The XRD diffractograms of synthesized hydroxyapatite at 140°C, 160°C, and 180°C, each for 20 hours, are depicted at Figure 5.

XRD analysis was conducted on synthesized hydroxyapatite at 2θ angles of 5–60°. The diffraction patterns of all synthesized samples corresponded well with the JCPDS 9-432 standard data for hydroxyapatite, confirming successful formation of the hexagonal crystal phase. The presence of high and narrow peak intensities across all samples indicates excellent crystallinity of the synthesized products (Dey et al. 2014).

A slight shift in 2θ angles was observed between the synthesized samples and the JCPDS 9-432 standard data. This deviation can be attributed to several factors inherent to the hydrothermal synthesis process. Variations in synthesis temperature may induce lattice strain or alter the unit cell parameters of the hydroxyapatite crystal, leading to a measurable shift in diffraction peak positions according to Bragg's law ($2d \sin\theta = n(\lambda)$. Furthermore, partial substitution of carbonate ions (CO_3^{2-}) at phosphate sites (type B substitution) can cause local lattice distortion, as CO_3^{2-} has a different ionic radius and geometry compared to PO_4^{3-}, resulting in contraction or expansion of the unit cell (Fleet and Liu 2007). Crystallite size effects may also contribute, as nanocrystalline materials often exhibit peak broadening and slight positional shifts due to incomplete long-range order. Despite these deviations, the overall diffraction patterns remained consistent with the hydroxyapatite standard, and no peaks corresponding to secondary phases were detected, confirming that the synthesized product is hydroxyapatite (Sirait et al. 2020).

Among the synthesis temperatures evaluated, samples synthesized at 140°C exhibited notably lower peak intensities at higher 2θ angles compared to those synthesized at 160°C and 180°C. This is attributed to incomplete crystal formation at lower temperatures, which results in reduced X-ray absorption and poorer crystallinity (Hokmabad et al. 2019). In contrast, higher synthesis temperatures promoted more complete crystal growth, as reflected by improved peak intensities at 160°C and 180°C. The crystallite size of the synthesized hydroxyapatite was calculated using the Scherrer equation:

$$D = \frac{K\lambda}{\beta \cos\theta} \quad (4)$$

where D is the crystallite size (nm), K is the shape factor (0.9), λ is the X-ray wavelength (Cu Kα radiation, λ = 0.15406 nm), β is the full width at half maximum (FWHM) of the selected diffraction peak expressed in radians, and θ is the Bragg angle. The FWHM values were obtained from peak fitting analysis, and β values were converted from degrees to radians prior to substitution into the Scherrer equation. The crystal size and crystallinity results are presented in Table 5.

As the temperature increases, the thermal energy in the system increases. This affects the reactivity of the phosphate and calcium ions in the solution. Increasing the temperature can increase the rate of reaction, which can accelerate the growth of hydroxyapatite crystals, resulting a higher crystallinity. However, hydroxyapatite synthesis has an optimum temperature where reaction conditions achieve optimum crystal formation. At the optimum temperature, crystals grow optimally, resulting in high crystallinity and the desired crystal size (Lee et al. 2020). As the atomic configuration of the substance becomes more structured, the percentage of crystallinity increases because of the increased temperature, facilitating the formation of additional crystals. When synthesis temperature exceeds the optimum, excessive thermal energy disrupts ionic equilibrium in solution, inhibiting further crystal nucleation and growth (Purnama and Langenati 2006). In addition, PO_4^{3-} ions can also decrease in intensity if they have passed the optimum temperature because they are substituted with CO_3^{2-} ions as the reaction temperature increases.

Based on the result above, the optimum temperature for hydrothermally synthesized hydroxyapatite is 160°C, with a crystal size of 14.50 nm and a crystallinity of 98.90%. This conclusion is supported by the highest yield and lowest carbonate content obtained at 160°C for each variation of the same reaction time. Hydroxyapatite with high crystallinity has better osteo-conductivity and osteointegration properties than lower crystallinity hydroxyapatite (Uskoković and Uskoković 2011). Additionally, research has shown that hydroxyapatite crystals ranging from 10 to 100 nm have better biocompatibility and osteogenic potential compared to larger crystals. This is due to the fact that smaller crystals provide a larger surface area for the interaction with bone cells, allowing a better integration with bone tissue (dos Anjos et al. 2019). Hydroxyapatite crystals over 100 nm might cause embolism and the crystals will get eliminated by the phagocytosis process. On the other hand, particles smaller than 10 nm will be easily

TABLE 5. Synthesized Hydroxyapatite Crystal Size and Crystallinity.

Temperature (°C)	Crystal Size (nm)	Crystallinity (%)
140	23.70	90.82
160	14.50	98.90
180	19.97	97.84

filtered by the kidneys, so the crystals will not remain in the body for a long time (Rajula et al. 2021).

3.5 Comparison Between Synthesized and Commercial Hydroxyapatite

To evaluate the potential of ale-ale shell-derived hydroxyapatite for biomedical applications, the physicochemical properties of the optimum synthesized product were compared against commercially available hydroxyapatite references and the ISO 13779 standard. In this study, the comparison focused on crystal size and crystallinity between the two types of hydroxyapatites. The data on commercial hydroxyapatite were taken from a comparative study conducted by Sobczak-Kupiec et al. (2012) and Giraldo-Betancur et al. (2013), which included five commercial hydroxyapatite samples, which were NIST, Sigma Aldrich, Merck, Coralina, and Habiocer hydroxyapatite. It should be noted that not all of these commercial hydroxyapatite types are intended for medical applications. All data will be compared to the international standard ISO 13779 on Clinical Implications and Testing of Bone Implant Products, especially in section 3 focusing on crystalline hydroxyapatite. The comparison of synthesized hydroxyapatite and commercial hydroxyapatite are presented in Table 6.

Based on the comparison in Table 6, the synthesized hydroxyapatite met the ISO 13779 standard, with a crystallinity of 98.90%, well above the minimum threshold of 45%, and a crystal size of 14.50 nm, which falls within the specified range. However, conformity with dimensional and crystallinity standards alone is insufficient to fully characterize the clinical potential of a bone graft material.

Beyond crystallinity and crystal size, a comprehensive assessment of hydroxyapatite suitability for bone graft applications requires consideration of additional parameters including biocompatibility, osteoconductivity, mechanical properties, and cost-effectiveness. With respect to biocompatibility, hydroxyapatite is generally recognized as a non-toxic and non-immunogenic material due to its chemical similarity to the inorganic phase of natural bone (Sadat-Shojai et al. 2013). The nano-scale crystal size obtained in this study (14.50 nm) is within the 10–100 nm range reported to favor cell adhesion, proliferation, and osteogenic differentiation, as smaller crystals provide a higher surface area-to-volume ratio for interaction with bone cells (dos Anjos et al. 2019; Rajula et al. 2021). Furthermore, the high crystallinity (98.90%) obtained at the optimum condition is associated with improved osteoconductivity and osseointegration, as highly crystalline HAp exhibits greater structural stability and slower degradation rate in physiological environments, allowing sufficient time for new bone ingrowth (Uskoković and Uskoković 2011).

From an economic standpoint, the use of ale-ale shells as a calcium precursor offers a significant cost advantage over synthetic or imported calcium sources. Ale-ale shells are an abundantly available shellfish waste in Kalimantan, Indonesia, and their utilization as a HAp precursor aligns with the principles of circular economy and waste valorization. While a formal cost analysis was beyond the scope of this study, the low-cost and locally available nature of the raw material suggests strong potential for reducing Indonesia's dependence on imported hydroxyapatite. Nevertheless, in vitro cytotoxicity testing, cell adhesion assays, and in vivo bone regeneration studies remain necessary to fully validate the biological performance of this material prior to any clinical application. These evaluations, together with a systematic cost-effectiveness analysis and scale-up feasibility study, are recommended as priorities for future research.

Several limitations of the present study should be acknowledged. Each synthesis condition was conducted as a single independent batch, therefore statistical validation was not performed. The reported values therefore represent single measurements per condition, and observed trends should be interpreted as indicative rather than statistically validated. Additionally, characterization was limited to FTIR and XRD; complementary analyses such as scanning electron microscopy (SEM) for morphological assessment, thermogravimetric analysis (TGA) for independent carbonate quantification, and BET surface area measurement would provide a more comprehensive physicochemical profile of the synthesized material. Furthermore, no biological evaluation was conducted in this study; in vitro cytotoxicity and cell adhesion assays remain necessary to confirm biocompatibility prior to any clinical consideration. Future work should incorporate replicate syntheses and broader characterization to strengthen the statistical validity and translational relevance of ale-ale shell-derived hydroxyapatite.

TABLE 6. Comparison between synthesized and commercial hydroxyapatite.

Characteristics	Synthesized Hap	NIST	Sigma	Merck	Coralina	Habiocer	ISO 13779
Crystal Size (nm)	14.50	149	149	153.3	149	12.93	2-200
Crystallinity (%)	98.90	83.35	91.76	95	84.07	90.10	45

4. CONCLUSIONS

This study demonstrates the feasibility of hydrothermally synthesizing hydroxyapatite ($Ca_{10}(PO_4)_6(OH)_2$) from ale-ale shells (*Meretrix meretrix*) as a sustainable and affordable calcium precursor. The calcined ale-ale shells exhibited a high calcium content of 94.42% and CaO content of 93.44%, confirming their suitability as a raw material for HAp synthesis. FTIR analysis confirmed the successful formation of hydroxyapatite, evidenced by the characteristic hydroxyl (OH^-) and phosphate (PO_4^{3-}) functional groups, with minor carbonate (CO_3^{2-}) impurities. The carbonate content across all conditions ranged from 1.00–1.52%, well below the 8% maximum allowable limit for bone implant applications and may be regarded as a biomimetically favorable characteristic rather than a critical impurity. XRD analysis confirmed the formation of hexagonal-phase hydroxyapatite consistent with the JCPDS 09-0432 standard, with characteristic diffraction peaks at 2θ values of 31.74°, 31.82°, and 31.76° for synthesis temperatures of 140°C, 160°C, and 180°C, respectively, corresponding to the (211) crystallographic plane.

The optimum reaction time was identified as 20 hours, yielding the highest product yield of 54.08% and the lowest carbonate impurity content of 1.00%. The optimum synthesis temperature was 160°C, producing hydroxyapatite with a nano-scale crystal size of 14.50 nm and crystallinity of 98.90%, both of which meet the ISO 13779 standard for crystalline hydroxyapatite. The physicochemical properties of the synthesized HAp are comparable to those of commercial hydroxyapatite, demonstrating the potential of ale-ale shell derived HAp as a viable, locally sourced alternative to imported products. The utilization of shellfish waste as a precursor aligns with circular economy principles and offers a promising pathway toward reducing Indonesia's dependence on imported biomaterials.

Future work should prioritize: (1) in vitro cytotoxicity and cell adhesion assays to confirm biocompatibility, (2) in vivo bone regeneration studies to evaluate osteoconductivity and osseointegration performance, (3) systematic cost-effectiveness and scale-up feasibility analyses to assess commercial viability, and (4) replicate synthesis studies with statistical validation to strengthen the robustness of the reported optimization trends.

5. ACKNOWLEDGEMENTS

This research was funded by the Program Kreativitas Mahasiswa – Riset Eksakta (PKM-RE), Directorate of Learning and Student Affairs, Ministry of Research, Technology and Higher Education of the Republic of Indonesia. The ale-ale shells (Meretrix meretrix) used in this study were obtained from post-harvest shellfish waste sourced from local fishermen in Ketapang, West Kalimantan, Indonesia. No living organisms were specifically collected for this research, and all shell materials were derived from existing post-harvest waste streams, thereby minimizing additional environmental impact. The authors declare no conflict of interest.

REFERENCES

Abifarin JK, Obada DO, Dauda ET, Dodoo-Arhin D. 2019. Experimental data on the characterization of hydroxyapatite synthesized from biowastes. Data in Brief. 26:104485. doi:10.1016/j.dib.2019.104485.

Anisah A, Delina M, Aisah N, Gustiono D. 2018. Pembuatan graft tulang dengan proses ekstraksi senyawa hidroksiapatit dari tulang korteks sapi. Spektra: Jurnal Fisika dan Aplikasinya. 3(1):31–36. doi:10.21009/spektra.031.05.

Azis Y, Jamarun N, Arief S, Nur H. 2015. Facile synthesis of hydroxyapatite particles from cockle shells (Anadara-granosa) by hydrothermal method. Oriental Journal of Chemistry. 31(2):1099–1105. doi:10.13005/ojc/310261.

Barrère F, van Blitterswijk CA, de Groot K. 2006. Bone regeneration: molecular and cellular interactions with calcium phosphate ceramics. International journal of nanomedicine. 1(3):317–332. https://pmc.ncbi.nlm.nih.gov/articles/PMC2426803/.

Berzina-Cimdina L, Borodajenko N. 2012. Research of calcium phosphates using fourier transform infrared spectroscopy. InTech. doi:10.5772/36942.

Castro MAM, Portela TO, Correa GS, Oliveira MM, Rangel JHG, Rodrigues SF, Mercury JMR. 2022. Synthesis of hydroxyapatite by hydrothermal and microwave irradiation methods from biogenic calcium source varying pH and synthesis time. Boletin de la Sociedad Espanola de Ceramica y Vidrio. 61(1):35–41. doi:10.1016/j.bsecv.2020.06.003.

Dey S, Das M, Balla VK. 2014. Effect of hydroxyapatite particle size, morphology and crystallinity on proliferation of colon cancer HCT116 cells. Materials Science and Engineering C. 39(1):336–339. doi:10.1016/j.msec.2014.03.022.

Directorate General of Capture Fisheries. 2021. Statistika perikanan tangkap indonesia. Kementrian perikanan dan kelautan indonesia. Technical report. Direktorat Jenderal Perikanan Tangkap. Jakarta.

dos Anjos S, Mavropoulos E, Alves GG, Costa AM, de Alencar Hausen M, Spiegel CN, Longuinho MM, Mir M, Granjeiro JM, Rossi AM. 2019. Impact of crystallinity and crystal size of nanostructured carbonated hydroxyapatite on pre-osteoblast in vitro biocompatibility. Journal of Biomedical Materials Research - Part A. 107(9):1965–1976. doi:10.1002/jbm.a.36709.

Earl JS, Wood DJ, Milne SJ. 2006. Hydrothermal synthesis of hydroxyapatite. Journal of Physics: Conference Series. 26(1):268–271. doi:10.1088/1742-6596/26/1/064.

Fadli A, Akbar F, Putri P, Pratiwi DI, Muhara I. 2014. Hydroxyapatite Powder Prepared by Low Temperature Hydrothermal Method from Sea Shells. International Society of Ocean, Mechanical and Aerospace Scientists and Engineers. 1(1):24–29. https://isomase.org/OMAse/Vol.1-2014/Section-4/4-5.pdf.

Featherstone JD, Pearson S, LeGeros RZ. 1984. An infrared method for quantification of carbonate in carbonated apatites1. Caries Research. 18(1):63–66. doi:10.1159/000260749.

Fleet ME, Liu X. 2004. Location of type B carbonate ion in type A-B carbonate apatite synthesized at high pressure. Journal of Solid State Chemistry. 177(9):3174–3182. doi:10.1016/j.jssc.2004.04.002.

Fleet ME, Liu X. 2007. Coupled substitution of type A and B carbonate in sodium-bearing apatite. Biomaterials. 28(6):916–926. doi:10.1016/j.biomaterials.2006.11.003.

Gheisari H, Karamian E, Abdellahi M. 2015. A novel hydroxyapatite -Hardystonite nanocomposite ceramic. Ceramics

International. 41(4):5967–5975. doi:10.1016/j.ceramint.2015.01.033.

Giraldo-Betancur AL, Espinosa-Arbelaez DG, Del Real-López A, Millan-Malo BM, Rivera-Muñoz EM, Gutierrez-Cortez E, Pineda-Gomez P, Jimenez-Sandoval S, Rodriguez-García ME. 2013. Comparison of physicochemical properties of bio and commercial hydroxyapatite. Current Applied Physics. 13(7):1383–1390. doi:10.1016/j.cap.2013.04.019.

Harahap AW, Helwani Z, Zultiniar, Yelmida. 2015. Sintesis hidroksiapatit melalui precipitated calcium carbonate (PCC) cangkang kerang darah dengan metode hidrotermal pada variasi Ph dan waktu reaksi. [[Doctoral thesis]]: Universitas Riau.

Hokmabad VR, Davaran S, Aghazadeh M, Rahbarghazi R, Salehi R, Ramazani A. 2019. Fabrication and characterization of novel ethyl cellulose-grafted-poly (ε-caprolactone)/alginate nanofibrous/macroporous scaffolds incorporated with nano-hydroxyapatite for bone tissue engineering. Journal of Biomaterials Applications. 33(8):1128–1144. doi:10.1177/0885328218822641.

Ishikawa T, Ogawa T. 2004. Coloring phenomenon of hydroxyapatite. Journal of the Ceramic Society of Japan. 112(1301):57–60. doi:10.2109/jcersj.112.57.

Johansson P, Jimbo R, Kozai Y, Sakurai T, Kjellin P, Currie F, Wennerberg A. 2015. Nanosized hydroxyapatite coating on peek implants enhances early bone formation: A histological and three-dimensional investigation in rabbit bone. Materials. 8(7):3815–3830. doi:10.3390/ma8073815.

Lee IH, Lee JA, Lee JH, Heo YW, Kim JJ. 2020. Effects of pH and reaction temperature on hydroxyapatite powders synthesized by precipitation. Journal of the Korean Ceramic Society. 57(1):56–64. doi:10.1007/s43207-019-00004-0.

LeGeros RZ. 2002. Properties of osteoconductive biomaterials: Calcium phosphates. Clinical Orthopaedics and Related Research. 395:81–98. doi:10.1097/00003086-200202000-00009.

Oktaviani A. 2019. Sintesis CaO dari cangkang kerang ale-ale (Meretrix meretrix) pada suhu kalsinasi 900oC. Jurnal Kimia Khatulistiwa. 8(1):37–40. https://jurnal.untan.ac.id/index.php/jkkmipa/article/view/32529.

Phatai P, Futalan CM, Utara S, Khemthong P, Kamonwannasit S. 2018. Structural characterization of cerium-doped hydroxyapatite nanoparticles synthesized by an ultrasonic-assisted sol-gel technique. Results in Physics. 10:956–963. doi:10.1016/j.rinp.2018.08.012.

Piccirillo C, Silva MF, Pullar RC, Braga Da Cruz I, Jorge R, Pintado MM, Castro PM. 2013. Extraction and characterisation of apatite- and tricalcium phosphate-based materials from cod fish bones. Materials Science and Engineering C. 33(1):103–110. doi:10.1016/j.msec.2012.08.014.

Purnama EF, Langenati SNR. 2006. Dibuat dengan media air dan cairan tubuh buatan (synthetic body fluid) preparasi pelarut sbf 1 liter identifikasi hidroksiapatit dengan XRD identifikasi hidroksiapatit dengan ftir. Jurnal Sains Materi Indonesia Indonesian Journal of Materials Science:154–159. https://repository.ipb.ac.id/handle/123456789/46346.

Purwasasmita BS, Gultom RS. 2008. Sintesis dan karakterisasi serbuk hidroksiapatit skala sub-mikron menggunakan metode presipitasi. Jurnal Bionatura. 10(2):155–167. https://jurnal.unpad.ac.id/bionatura/article/view/7734.

Rachmantio C, Irfai MA. 2023. Pengaruh suhu dan waktu kalsinasi terhadap kemurnian hidroksiapatit berbasis cangkang kerang hijau untuk aplikasi pada bone tissue engineering. Jtm. 11(1):1–6. https://ejournal.unesa.ac.id/index.php/jtm-unesa/article/view/50689.

Rajula M, Narayanan V, Venkatasubbu G, Mani R, Sujana A. 2021. Nano-hydroxyapatite: A driving force for bone tissue engineering. Journal of Pharmacy and Bioallied Sciences. 13(5):S11–S14. doi:10.4103/jpbs.JPBS_683_20.

Ryu GU, Kim GM, Khalid HR, Lee HK. 2019. The effects of temperature on the hydrothermal synthesis of hydroxyapatite-zeolite using blast furnace slag. Materials. 12(13):2131. doi:10.3390/ma12132131.

Sadat-Shojai M, Khorasani MT, Dinpanah-Khoshdargi E, Jamshidi A. 2013. Synthesis methods for nanosized hydroxyapatite with diverse structures. Acta Biomaterialia. 9(8):7591–7621. doi:10.1016/j.actbio.2013.04.012.

Sahadat Hossain M, Ahmed S. 2023. FTIR spectrum analysis to predict the crystalline and amorphous phases of hydroxyapatite: a comparison of vibrational motion to reflection. RSC Advances. 13(21):14625–14630. doi:10.1039/d3ra02580b.

Sirait M, Sinulingga K, Siregar N, Siregar RSD. 2020. Synthesis of hydroxyapatite from limestone by using precipitation method. Journal of Physics: Conference Series. 1462(1):012058. doi:10.1088/1742-6596/1462/1/012058.

Sobczak-Kupiec A, Malina D, Kijkowska R, Wzorek Z. 2012. Comparative study of hydroxyapatite prepared by the authors with selected commercially available ceramics. Digest Journal of Nanomaterials and Biostructures. 7(1):385–391. https://chalcogen.ro/385_Kupiek.pdf.

Sulistyawati E, Siregar RFS. 2019. Karakteristik hidroksiapatit porous dari prekursor cangkang keong sawah dan bahan porogen pati sukun. Eksergi. 16(2):59. doi:10.31315/e.v16i2.3082.

Tang W, Xu W, Zhong M, Zhang Z. 2023. Slightly doped hydroxyapatite pigments of subtractive color with high near-infrared reflectance. Journal of Solid State Chemistry. 322:123947. doi:10.1016/j.jssc.2023.123947.

Uskoković V, Uskoković DP. 2011. Nanosized hydroxyapatite and other calcium phosphates: Chemistry of formation and application as drug and gene delivery agents. Journal of Biomedical Materials Research - Part B Applied Biomaterials. 96 B(1):152–191. doi:10.1002/jbm.b.31746.

Yusuf Y. 2021. Karbonat hidroksiapatit dari bahan alam: pengertian, karakterisasi, dan aplikasi. Yogyakarta: UGM Press, Universitas Gadjah Mada.

Zhu Y, Xu L, Liu C, Zhang C, Wu N. 2018. Nucleation and growth of hydroxyapatite nanocrystals by hydrothermal method. AIP Advances. 8(8). doi:10.1063/1.5034441.